ChemPhysChem

Research Article
doi.org/10.1002/cphc.202200735

Chemistry Europe
European Chemical
Societies Publishing

www.chemphyschem.org

Effects of Heavy Iodine Atoms and π-Expanded Conjugation on Charge Transfer Dynamics in Carboxylic Acid BODIPY Derivatives as Triplet Photosensitizers

Elif Akhuseyin Yildiz,*[a] Ebru Yabaş,*[b] Fazlı Sözmen,[c] Yasemin Bozkurt,[d] Ahmet Karatay,[a] Bahadir Boyacioglu,[e] Hüseyin Ünver,[f] and Ayhan Elmali[a]

Borondipyrromethene (BODIPY) chromophores are composed of a functional-COOH group at meso position with or without a biphenyl ring, and their compounds with heavy iodine atoms at −2, −6 positions of the BODIPY indacene core were synthesized. The photophysical properties of the compounds were studied with steady-state absorption and fluorescence measurements. It was observed that the absorption band is significantly red-shifted, and fluorescence signals are quenched in the presence of iodine atoms. In addition to that, it was indicated that the biphenyl ring does not affect the spectral shifting in the absorption as well as fluorescence spectra. In an attempt to investigate the effect of π-expanded biphenyl moieties and heavy iodine atoms on charge transfer dynamics, femtosecond

transient absorption spectroscopy measurements were carried out in the environment of the tetrahydrofuran (THF) solution. Based on the performed ultrafast pump-probe spectroscopy, BODIPY compounds with iodine atoms lead to intersystem crossing (ISC) and ISC rates were determined as 150 ps and 180 ps for iodine BODIPY compounds with and without π-expanded biphenyl moieties, respectively. According to the theoretical results, the charge transfer in the investigated compounds mostly appears to be intrinsic local excitations, corresponding to high photoluminescence efficiency. These experimental findings are useful for the design and study of the fundamental photochemistry of organic triplet photosensitizers.

Introduction

Triplet photosensitizers have recently attracted much attention due to their being widely used in photodynamic therapy,[1–6] photocatalysis[7–9] and triplet-triplet annihilation-assisted upconversion mechanism.[10–12] The triplet photosensitizers and their applications include fundamental photophysical processes such as intersystem crossing (ISC), an electron and/or energy transfer mechanism. Conventionally produced triplet photosensitizers are limited to porphyrin, perylene chromophores and their metal complexes, Pt (II), Pd (II) or Zn (II)[13,14] and some halogenated dyes.[15,16] However, these chromophores have difficulties in preparation or purification, weak absorption bands

in the visible region, and loss of ISC upon derivation and functionalization of the molecules.

BODIPY chromophores can serve as organic-based triplet photosensitizers due to their demonstrating strong absorption in the visible spectrum, excellent photostability, and long-lived triplet excited states.[1,17,18] The wide range of applications can be associated with the tunability of the BODIPY sensitizer absorption spectrum coupled with its ability to form a triplet excited state by altering structural modification.[19,20] Triplet state formation is the main key for BODIPY to make them triplet photosensitizers, and different molecular schemes have been demonstrated for promoting BODIPY triplet state formation.[1,18,19,21–27] However, there have been limited studies focusing on how conjugation length with —COOH functional group affects the photophysical properties as well as the ISC mechanism in halogenated iodine BODIPY's.[28]

In this work, BODIPY chromophores with and without π-expanded biphenyl moieties and their compounds with iodine atoms were designed and synthesized. The BODIPY core, due to its electronic structure, tends to give electrophilic substitution reactions, especially from the 2- and 6-positions. BODIPY derivatives are often halogenated from these positions to yield various photosensitizers. This halogen-induced heavy atom effect leads to efficient intersystem crossing due to spin-orbit coupling. Iodine is a heavier atom than bromine and generally iodinated BODIPY compounds have higher singlet oxygen ($^1O_2$) quantum yields than the brominated BODIPY compounds.[29] Therefore, the main aim of this work is to investigate the effects of heavy iodine atoms as well as π-expanded biphenyl moieties with —COOH functional group on steady-state absorption,

[a] Dr. E. Akhuseyin Yildiz, Dr. A. Karatay, Dr. A. Elmali
Department of Physics Engineering, Faculty of Engineering, Ankara University, 06100 Beşevler-Ankara, Türkiye
E-mail: eakhuseyin@ankara.edu.tr

[b] Dr. E. Yabaş
Advanced Technology Application and Research Center, Sivas Cumhuriyet University, 58140 Sivas, Türkiye
E-mail: eyabas@cumhuriyet.edu.tr

[c] Prof. F. Sözmen
Nanotechnology Engineering Department, Faculty of Engineering, Sivas Cumhuriyet University, 58140 Sivas, Türkiye

[d] Dr. Y. Bozkurt
Department of Metallurgical and Materials Engineering, Sivas Cumhuriyet University, 58140 Sivas, Türkiye

[e] Prof. B. Boyacioglu
Vocational School of Health Services, Ankara University, 06290 Kecioren-Ankara, Türkiye
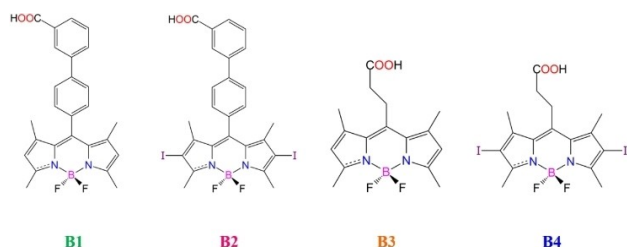
[f] Prof. H. Ünver
Department of Physics, Faculty of Science, Ankara University, 06100 Besevler-Ankara, Türkiye

ChemPhysChem

Research Article
doi.org/10.1002/cphc.202200735

**Chemistry
Europe**
European Chemical
Societies Publishing

emission, and charge transfer dynamics. The observed emission quenching was investigated and ISC processes were confirmed for iodinated BODIPY compounds by a femtosecond transient optical spectroscopic method in the visible region. In addition, as a contribution to the experimental study, we performed a theoretical study based on the density functional theory (DFT) method for the optical and electronic properties of the investigated compounds.

Results and Discussion

Steady-state absorption and fluorescence measurements

The dye molecules are made up of a functional-COOH group at meso position with or without a biphenyl ring and their compounds with heavy iodine atoms at -2, -6 positions of the BODIPY indacene core indicated in Scheme 1. The normalized linear absorption spectra of compounds **B1**, **B2**, **B3** and **B4** in THF solution are presented in Figure 1. Compounds **B1** and **B3** possessing substituents only in the meso position of the BODIPY core demonstrate strong absorption maxima at 500 nm with a shoulder around 470 nm wavelength, as shown in Figure 1. The observed strong absorption at 500 nm is the signature absorption of the BODIPY chromophore. Compounds **B2** and **B4** with substituents in the meso position and iodine atoms in the -2, -6 positions of the indacene BODIPY core, on
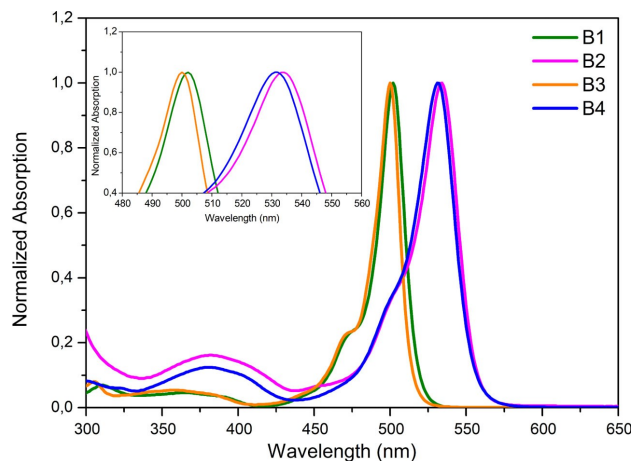
the other hand, have a strong absorption band around 530 nm and an insensible shoulder around 500 nm. The strong absorption bands around 500 nm and 530 nm correspond to the $S_0 \rightarrow S_1$ transition, while the absorption band in the shorter wavelength region between 325 nm and 450 nm correspond to $S_0 \rightarrow S_2$ transitions for all studied compounds. In the presence of iodine atoms, it was oserved that the main absorption signal shifted to the red region of the spectrum at about 30 nm.[23,30,31] This remarkable red shift originated from the intramolecular charge transfer character of the S_1 state because of the strong coupling between the highest occupied molecular orbitals of BODIPY and iodine atoms.

The fluorescence spectra of the BODIPY compounds with 2.5×10^{-5} M in THF solution are indicated in Figure 2. It is seen from the figure that compounds **B1** and **B3** with $-$COOH substituents are highly fluorescent compounds. The maximum intensity of the fluorescence signals is localized around 521 nm for compound **B1** and 518 nm for compound **B3** at 502 nm and 500 nm excitation wavelengths, respectively. This negligible red shift originated from the biphenyl ring on compound **B1**. The presence of an extra biphenyl ring leads to an increase in the charge transfer characteristic of the molecule and a decrease in the fluorescence intensity. Therefore, the emission intensity of compound **B1** is lower than that of compound **B3**. Besides, as shown in Figure 2 inset, the fluorescence emission spectrum of compounds **B1** and **B3** overlaps partially with their absorption spectra. Thus, it can be supposed that an energy transfer process takes place in the BODIPY–COOH system in which $-$COOH acts as the donor and BODIPY is the acceptor. On the other hand, attaching the iodine atoms to -2, -6 positions of indacene BODIPY caused fluorescence quenching for compounds **B2** and **B4** due to the heavy iodine atoms. In addition, a red-shift was observed in the emission wavelength depending on the iodine atoms in the BODIPY compounds as compared to compounds **B1** and **B3**. In an attempt to explain the fluorescence quenching mechanisms and investigate charge
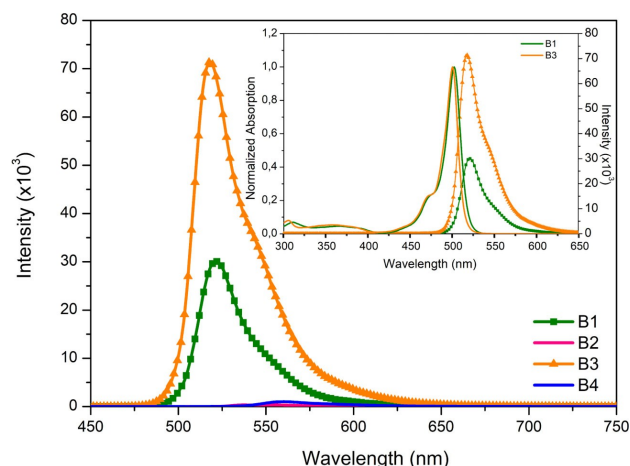

Scheme 1. Schematic illustration of the BODIPY sensitizers.

Figure 1. Normalized UV − vis absorption spectra of compounds **B1**, **B2**, **B3** and **B4** in THF solution.

Figure 2. Fluorescence spectra of compounds **B1**, **B2**, **B3** and **B4** in THF solution. The inset shows the absorption (normalized) and fluorescence spectra of **B1** and **B3** compounds in THF solution.

ChemPhysChem

Research Article
doi.org/10.1002/cphc.202200735

**Chemistry
Europe**
European Chemical
Societies Publishing

transfer dynamics, ultrafast pump-probe spectroscopy measurements were carried out.

Femtosecond Transient Absorption Spectroscopy Studies

Ultrafast pump-probe spectroscopy experiments were carried out to reveal the charge transfer dynamics as well as the decay kinetics of the BODIPY compounds in the THF environment. Upon pulsed laser excitation at 500 nm, the transient absorption spectra of compounds **B1** and **B3** are given in Figures 3a and 3c, respectively. Although there are minor differences, compounds **B1** and **B3** both demonstrate similar characteristics in their ultrafast pump-probe data. In transient absorption spectra of compounds **B1** and **B3**, there is a narrow negative absorption signal at 505 nm corresponding to ground state bleaching (GSB) with a tail lying around 600 nm that can be ascribed to stimulated emission (SE). This bleaching signal represents the depletion of singlet excited states, while the SE reflects the emission signal of the BODIPY compounds. The 505 nm bleaching signal decreases from the initial time delay until 3 ns as indicated in Figures 3a and 3c. On the other hand, there are positive signals localized above 460 nm, which can be ascribed to excited-state absorption (ESA) in the ultrafast pump-probe spectra representing transient absorptions for compounds **B1** and **B3**. The absorption around the 460 nm

region occurring simultaneously with the pump pulse is attributed to the $S_1 \rightarrow S_n$ transition of the —COOH–BODIPY moiety.

In the transient absorption spectra of compounds **B2** and **B4**, there is a GSB signal of around 538 nm with a shoulder of around 580 nm that can be attributed to the SE signal as seen in Figures 3b and 3d. In addition, the GSB signal shows negligible blue shifting with a time delay, as seen in Figures 3b and 3d. The reason for the blue shifting is the competition of the GSB signal with the ESA signal localized around 450 nm wavelength, appearing with a time delay in transient absorption spectra. In addition, there is a broad ESA signal rising between 560 nm and 800 nm with a time delay. Although there is no absorption signal at the initial time delay in this spectral region, it is observed that the amplitude of the positive signal increases with increasing time delay. The increment of the ESA signal with a longer time delay can be attributed to $T_1 \rightarrow T_n$ absorption via the intersystem crossing (ISC) mechanism. ISC is favoured in **B2** and **B4** compounds since the two iodine atoms are directly attached to the BODIPY skeleton. The presence of two iodine atoms at -2, -6 positions of the BODIPY core allows it to populate the lowest triplet excited state.

To reveal the kinetics of the photophysical processes, the decay traces at a few critical probe wavelengths were monitored and fitted by using a multiexponential fitting function. For both compounds **B1** and **B3**, the fast development
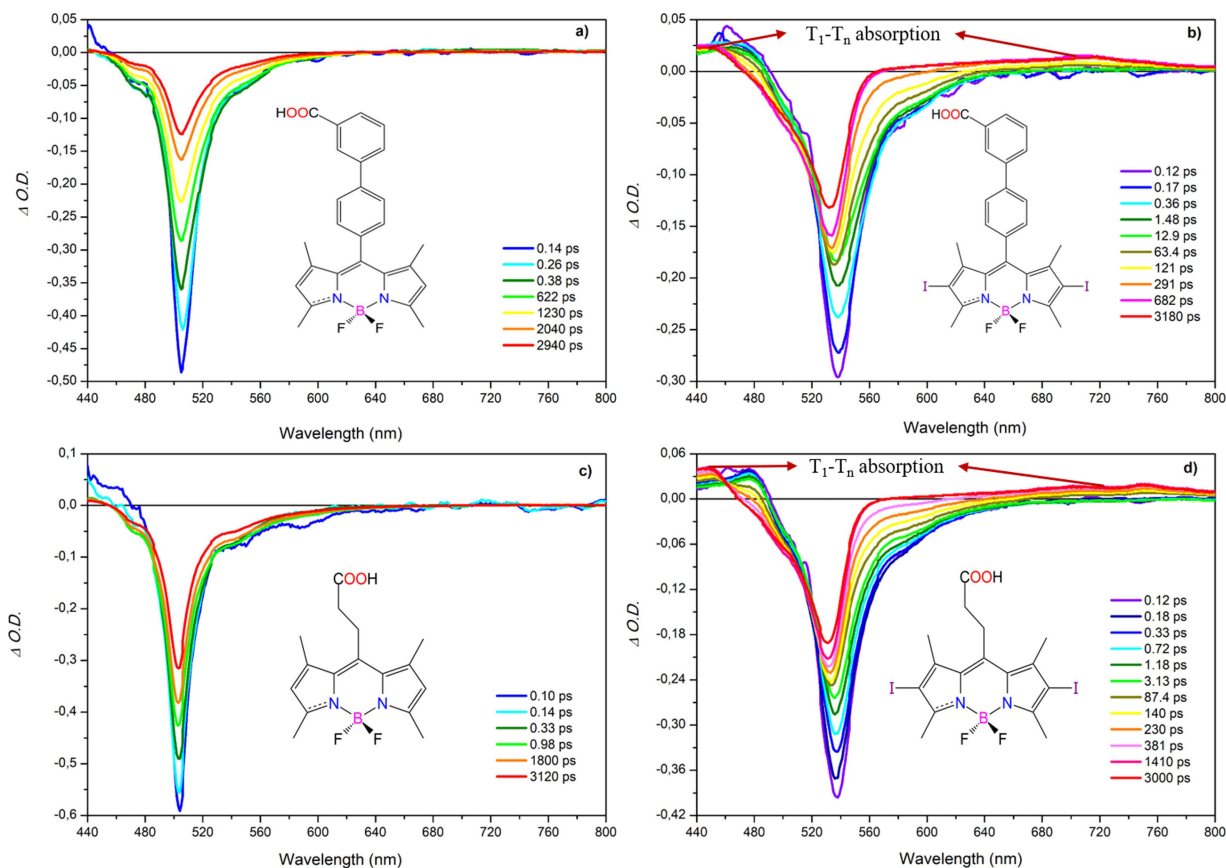

Figure 3. Transient absorption spectra of compounds a) **B1**, b) **B2**, c) **B3** and d) **B4** compounds in THF with different time delay, $\lambda_{ex} = 500$ nm and 530 nm.
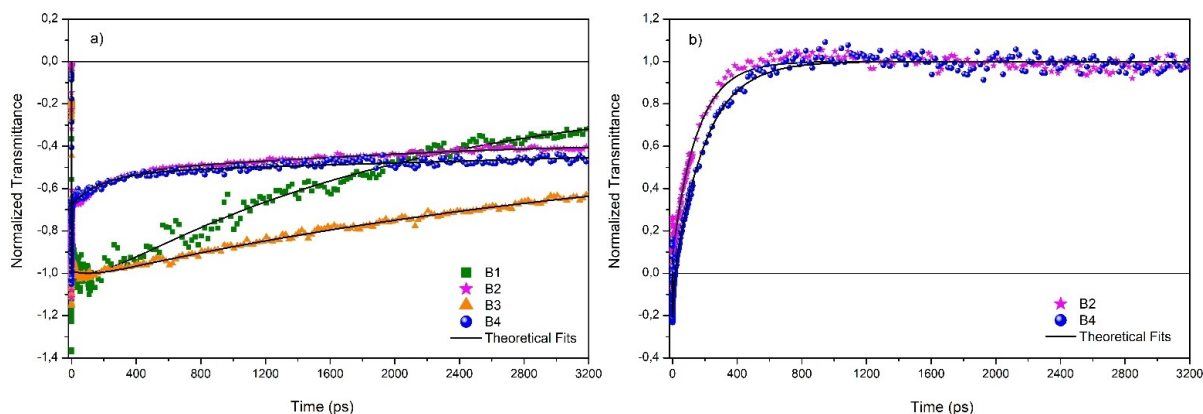
Figure 4. a) Time evolution of the bleach signals for compounds **B1**–**B4** in THF, b) Comparison of decay curves of compounds **B2** and **B4** at 716 nm and 705 nm probe wavelength, respectively.

of the bleaching at 505 nm is due to the prompt excitation of the COOH-BODIPY unit upon femtosecond laser excitation, while the slow component is associated with the charge recombination (Figure 4a). As seen from the figure, the decay traces of compound **B1** are slightly different from those of **B3** in terms of the lifetime of the bleaching signals at 505 nm. Compound **B1** demonstrates a faster time component and therefore more efficient intermolecular charge transfer due to the biphenyl rings. This result may be the reason compound **B3** has greater fluorescence intensity than compound **B1**, as indicated in fluorescence measurements (Figure 2). On the other hand, the decay traces of bleach signals of compounds **B2** and **B4** around 530 nm probe wavelength are also presented in Figure 4a and there is no remarkable distinction between these chromophores. The transient absorption spectrum of compounds **B2** and **B4** have three positive signals around 450 nm, 475 nm and in the range of 560 nm–800 nm. The ESA signal around 475 nm could be related to the $S_1 \rightarrow S_n$ transition of the –COOH group with a short lifetime, while the 450 nm and broad ESA signals appear after a long time delay due to the presence of iodine atoms. The lifetimes of these signals are long, and therefore these signals can be attributed to $T_1 \rightarrow T_n$ transitions. To extract the ISC rates, the probe wavelength around 720 nm was fitted and the ISC rates were found to be 150 ps and 180 ps for compounds **B2** and **B4**, respectively, as seen in Figure 4b.

DFT calculations

In this study, we have performed the electronic structure, optical absorption properties and DOS analysis of the investigated compounds using the DFT method. We have theoretically calculated UV-Visible spectra, FMOs analysis, global chemical reactivity descriptors, and the binding energies. These results are given in Table 1. The UV-Vis spectra that arise from electron excitation play a crucial role in understanding the optical sensing capabilities of the molecule. In Figure 5, we
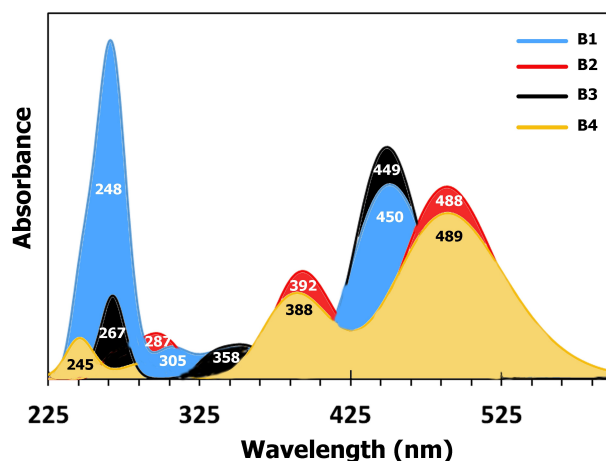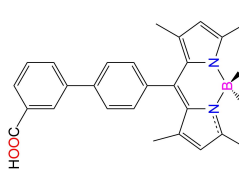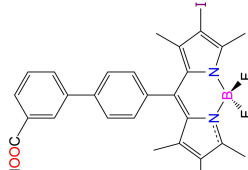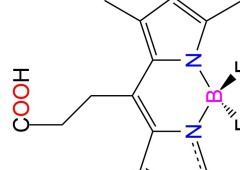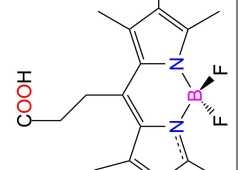

Figure 5. Theoretical UV-Vis spectra of compounds **B1**–**B4** in THF solvent.

present the UV-Vis spectra of the investigated compounds in THF solvent. Compound B1 has the highest absorbance at 450 nm (HOMO to LUMO electronic transitions with a 98% contribution), 305 nm (H-1 to L+1 with a 93% contribution), and 267 nm (H-1 to L+2 and H-6 to LUMO with 61% and 31% contributions, respectively), with excitation energies of 2.75, 4.06, and 4.65 eV. We have obtained the maximum absorbance values of dominant transitions for compound **B2** at 488 nm (HOMO to LUMO with 96% contribution), 392 nm (H-2 to LUMO and H-3 to LUMO with 83% and 12% contribution), 287 nm (H-8 to LUMO with 90% contribution) and 268 nm (HOMO to L+5 and HOMO to L+4 with 57% and 39% contribution), where the excitation energies of these values are 2.54, 3.16, 4.32 and 4.62 eV, respectively. In compound **B3**, λ_{abs} values are at 449 nm (HOMO to LUMO with 98% contribution), 358 nm (H-1 to LUMO with 97% contribution), and 267 nm (H-3 to LUMO with 88% contribution), where the excitation energies of these values are 2.76, 3.46 and 5.84 eV, respectively. Compound **B4** has excitation energies of 2.54, 3.19, and 5.05 eV at the maximum absorbances of 489 nm (HOMO to LUMO with 96% contribution), 388 nm (H-2 to LUMO with 96% contribution), and

Table 1. Frontier molecular orbitals, global chemical reactivity descriptors and optical properties of compounds **B1**–**B4**.

SOLVENT: THF COMPOUNDS	Theoretical λ_{abs} [nm]	Oscillator Strength f	Major contribution	E_{exc} [eV]	E_{HOMO} [eV]	E_{LUMO} [eV]	E_g [eV]	E_b [eV]	η [eV]	χ [eV]	ω [eV]
1	450 305 248	0.73 0.11 0.41	HOMO→LUMO (98%) H-1→L+1 (93%) H-5→L+1 (64%) H-1→L+2 (13%)	2.75 4.06 5.00	−5.88	−2.87	3.01	0.26	1.51	4.38	14.40
2	488 392 287	0.72 0.29 0.10	HOMO→LUMO (96%) H-2→LUMO (83%) H-3→LUMO (12%) H-8→LUMO (90%)	2.54 3.16 4.32	−6.03	−3.14	2.89	0.35	1.45	4.59	15.19
3	449 358 267	0.73 0.10 0.26	HOMO→LUMO (98%) H-1→LUMO (97%) H-3→LUMO (88%)	2.76 3.46 5.84	−5.91	−2.87	3.04	0.28	1.52	4.39	14.65
4	489 388 245	0.73 0.30 0.18	HOMO→LUMO (96%) H-2→LUMO (96%) H-8→LUMO (90%)	2.54 3.19 5.05	−6.06	−3.17	2.89	0.35	1.45	4.62	15.36

ChemPhysChem

Research Article
doi.org/10.1002/cphc.202200735

**Chemistry
Europe**
European Chemical
Societies Publishing

245 nm (H-8 to LUMO with 90% contribution), respectively. It seems that theoretical results agree well with the experimental data.

FMOs, also known as HOMOs (green discrete vertical line) and LUMOs (red discrete vertical line), are prominent for explaining chemical reactivity and the ability of a molecule to absorb light. Figures 6 a), b), c), and d) show the isosurfaces of HOMO and LUMO, with green lobes indicating negative and red lobes indicating positive, as well as the energy gap between HOMO and LUMO for compounds **B1**, **B2**, **B3** and **B4**, respectively. In addition, it is also clear from Table 1 that the HOMO-LUMO energy gaps ($E_g = |E_{HOMO} - E_{LUMO}|$) in THF solvent are 3.01, 2.89, 3.04 and 2.89 eV for compounds **B1**, **B2**, **B3** and **B4** respectively. Since the energy gaps of compounds **B2** and **B4** are small, the electrons more easily transition from HOMO to LUMO. Furthermore, GCRDs of the investigated compounds such as chemical hardness (η), electronegativity (χ), and electrophilicity (ω) indices may be derived using HOMO and LUMO energy values as follows:[32]

$$\eta = \frac{1}{2}(E_{LUMO} - E_{HOMO}), \ \chi = -\frac{1}{2}(E_{LUMO} + E_{HOMO}) \ , \ \omega = \frac{\chi^2}{2\eta} \quad (1)$$

Moreover, Table 1 shows that the chemical hardness values for compounds **B1**, **B2**, **B3** and **B4** are 1.51, 1.45, 1.52, and 1.45 eV, and the electronegativity values are 4.38, 4.59, 4.39 and 4.62 eV and the electrophilicity is 14.40, 15.19, 14.65 and 15.36 eV, respectively, using equation 1. Compounds **B2** and **B4** are thought to have lower excitation energies for many excited states, significant chemical reactivity, and are more reactive and softer molecules since they have smaller energy gap values. This suggests that compounds **B2** and **B4** can be photochemically excited. Since compounds **B2** and **B4** contain the highly electronegative iodine atom (I), they will attract all electrons towards themselves. Compounds **B2** and **B4** are stronger electrophiles than compound **B1**, which means they can attract more electrons than the others.[33,34] This means that the higher the HOMO energy, the easier it is for HOMO to give electrons. However, when the LUMO energy is low, it makes it easier for the LUMO to accept electrons.[35,36] Another way to determine
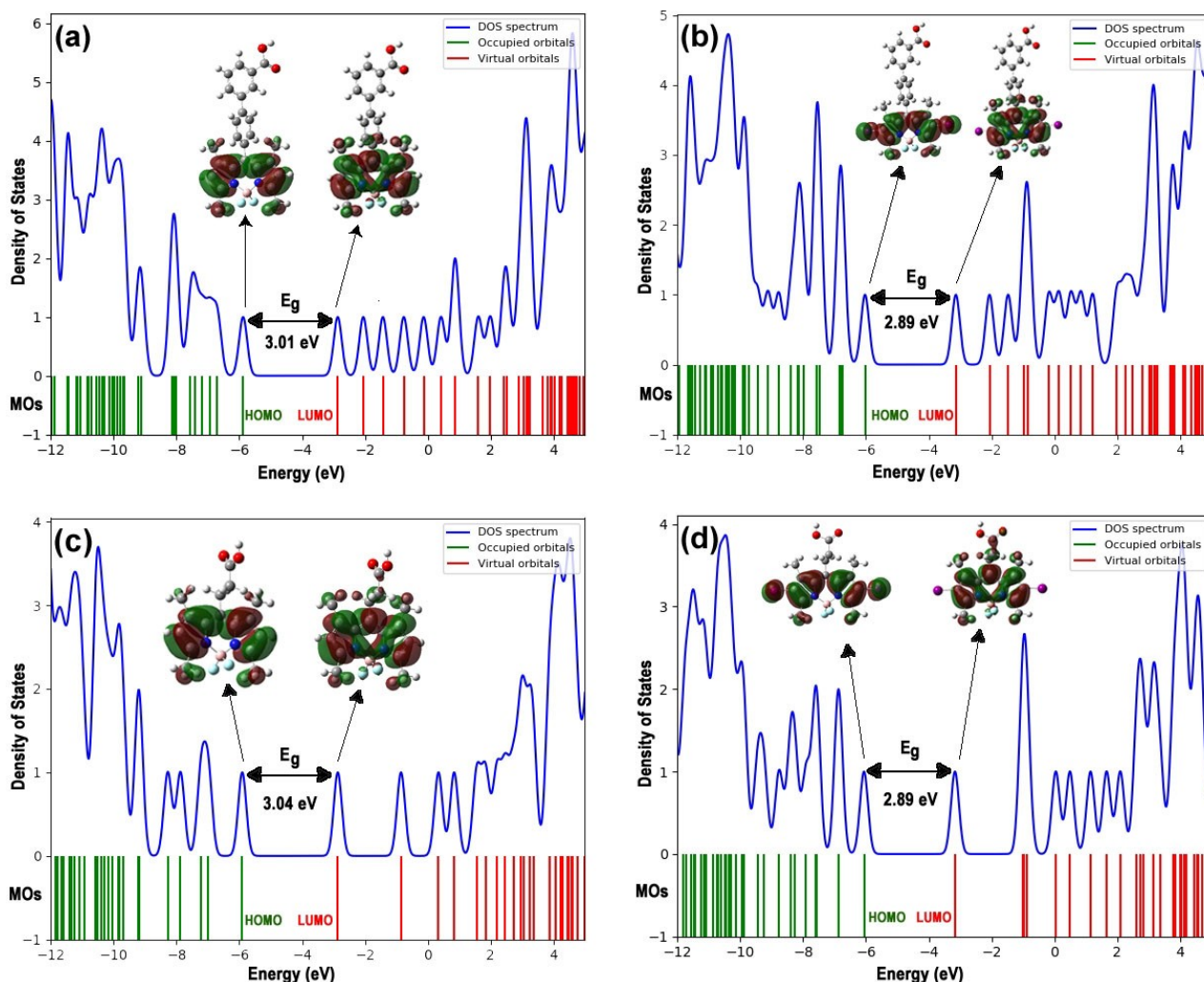

Figure 6. DOS and MOs spectra of compounds **B1**–**B4** in THF solvent: a) compound **B1**, b) compound **B2**, c) compound **B3** and d) compound **B4**.

ChemPhysChem

Research Article
doi.org/10.1002/cphc.202200735

**Chemistry
Europe**
European Chemical
Societies Publishing

the evaluation of optoelectronic properties is by the calculation of the binding energy (E_b). It is known that E_b contributes to the breakdown of the Coulomb attraction between the hole and the electron. E_b can be defined as follows:[37,38]

$$E_b = E_g - E_{exc} \tag{2}$$

where E_g is the HOMO-LUMO energy gap and E_{exc} is the lowest excitation energy in equation 2. It is clear from Table 1 that since compounds **B2** and **B4** have large binding energies, they can be direct bandgap materials and show great promise in optoelectronic applications.
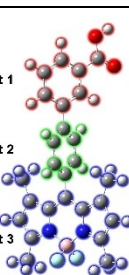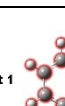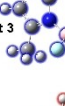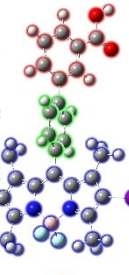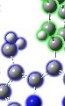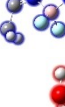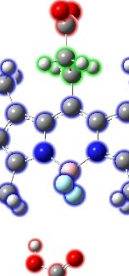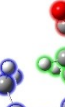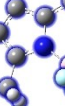
Considering only the HOMO and LUMO may not result in a realistic description of the boundary orbitals. Many studies have shown that DOS gives appropriate explanations for the features of charge transport.[37,39] The DOS diagrams are most commonly used to show MO compositions and their contributions to chemical bonding via positive and negative charges.[35]

Similarly, DOS diagrams (blue line) of the investigated compounds are presented in Figures 6a), b), c) and d). It can be

concluded that the presence of slightly more occupied energy levels in the virtual orbitals of compound **B4** implies that the sensing ability is somewhat greater than the others.[34]

Inter-fragment charge transfer (IFCT) is another method for determining charge transfer in the electron excitation process.[40] Here we have calculated the amount of c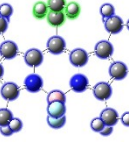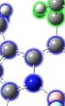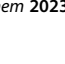harge transfer between different fragments. We have also computed the charge transfer percentage (CT%) and its complement local excitation percentage (LE%) are frequently involved in electron excitation studies between the three fragments we identified in compounds **B1**–**B4** for $S_0 \rightarrow S_1$ transitions having the maximum oscillator strength. The results are very easy to understand from Table 2. The results show that during the $S_0 \rightarrow S_1$ excitation, it is seen that there is no charge transfer between fragments in all compounds. Since the value of LE(%) is significantly larger than the value of CT(%) for all compounds, we can say that these excitations can be mostly regarded as the intrinsic local excitation. That is, these excitations are a local excitation of the acceptor moiety since there is an overlap between hole and electron, where both can be located in the acceptor fragment.

Table 2. IFCT analysis for compounds **B1**–**B4** for electronic transition $S_0 \rightarrow S_1$ in THF solvent.

Compounds	Transferred electrons between fragments			CT%	LE%
B1	$1 \rightarrow 2 : 0.00$ $1 \leftarrow 2 : 0.00$ *Net* $: 0.00\ (1 \rightarrow 2)$	$1 \rightarrow 3 : 0.00$ $1 \leftarrow 3 : 0.00$ *Net* $: 0.00\ (1 \rightarrow 3)$	$2 \rightarrow 3 : 0.00$ $2 \leftarrow 3 : 0.02$ *Net* $: -0.02\ (2 \rightarrow 3)$	3	97
B2	$1 \rightarrow 2 : 0.00$ $1 \leftarrow 2 : 0.00$ *Net* $: 0.00\ (1 \rightarrow 2)$	$1 \rightarrow 3 : 0.00$ $1 \leftarrow 3 : 0.00$ *Net* $: 0.00\ (1 \rightarrow 3)$	$2 \rightarrow 3 : 0.00$ $2 \leftarrow 3 : 0.02$ *Net* $: -0.02\ (2 \rightarrow 3)$	3	97
B3	$1 \rightarrow 2 : 0.00$ $1 \leftarrow 2 : 0.00$ *Net* $: 0.00\ (1 \rightarrow 2)$	$1 \rightarrow 3 : 0.00$ $1 \leftarrow 3 : 0.00$ *Net* $: -0.00\ (1 \rightarrow 3)$	$2 \rightarrow 3 : 0.00$ $2 \leftarrow 3 : 0.02$ *Net* $: -0.02\ (2 \rightarrow 3)$	3	97
B4	$1 \rightarrow 2 : 0.00$ $1 \leftarrow 2 : 0.00$ *Net* $: 0.00\ (1 \rightarrow 2)$	$1 \rightarrow 3 : 0.00$ $1 \leftarrow 3 : 0.01$ *Net* $: -0.01\ (1 \rightarrow 3)$	$2 \rightarrow 3 : 0.00$ $2 \leftarrow 3 : 0.02$ *Net* $: -0.02\ (2 \rightarrow 3)$	4	96

ChemPhysChem

Research Article
doi.org/10.1002/cphc.202200735

Chemistry Europe
European Chemical
Societies Publishing

Experimental Section

Synthesis of B1

Compound **B1** was synthesized according to the literature.[41] The synthesis procedure is briefly as follows. To a 500 mL round-bottomed flask containing 250 mL argon-degassed dichloromethane, 2,4-dimethylpyrrole (1.94 mmol, 184 mg), 4'-formylbiphenyl-3-carboxylic acid (0.88 mmol, 200 mg) and a drop of TFA were added, respectively. The reaction was allowed to stir overnight at room temperature. Then, DDQ (0.88 mmol, 199.76 mg) was added and stirred for one additional hour. After that, triethylamine (5 mL) was added and stirred for one additional hour and bortrifluoride diethylether compounds ($BF_3.OEt_2$) (3 mL) were added and the reaction mixture was left to stir at room temperature for 1 h. When the starting material was consumed, water (100 mL) was added and the reaction mixture was extracted with DCM (3x100 mL) and the organic phase was dried over $MgSO_4$. The organic solvent was removed under reduced pressure. The final product was purified on a flash silica column using an ethyl acetate/hexane (5 : 1, v/v) solvent system (28%).

Synthesis of B2

Compound **B2** was synthesized according to the literature.[41] Firstly, compound **B1** (0.122 mmol, 54 mg) and I_2 (0.244 mmol, 69.25 mg) were dissolved in ethanol (100 mL). Then Iodic acid (HIO_3), (0.244 mmol, 42.92 mg) was dissolved in a few drops of water and was added to this solution. The reaction mixture was stirred at room temperature. When the starting material was consumed, saturated sodium thiosulfate solution was added (50 mL) and extracted with DCM. The organic phase was then extracted twice more with water. The combined organic phase was dried over $MgSO_4$ and evaporated under reduced pressure. The crude product was purified by silica gel column chromatography using ethyl acetate/hexane (5 : 1, v/v) as the eluant (45%).

Synthesis of B3

Compound **B3** was synthesized according to the literature.[42] At first, 2,4-dimethyl pyrrole (1.0 mL, 10 mmol), succinic anhydride (400 mg, 4.0 mmol), and $BF_3.OEt_2$ (0.50 mL, 4.0 mmol) was added to 30 mL of toluene. The reaction mixture was heated to 80 °C and stirred under a nitrogen atmosphere for 5 h. Then the reaction mixture was cooled to room temperature and $BF_3.OEt_2$ (5.0 mL, 4.0 mmol) and triethylamine (Et_3N) (10 mL, 80 mmol) were added. The mixture was stirred for an additional 16 h at room temperature under a nitrogen atmosphere. After that, the reaction was quenched with 60 mL of 0.1 M HCl aqueous solution. Then the mixture was extracted with DCM and the organic phase was washed twice with water. The obtained organic fractions were combined and dried over magnesium sulfate ($MgSO_4$). The organic solvent was removed under reduced pressure and the product was purified with a flash silica column using 85% ethylacetate:hexane, (v/v) as the eluant (20%).

Synthesis of B4

Compound **B4** was synthesized according to the literature.[42] Firstly, compound **B3** (600 mg, 1.87 mmol) was dissolved in 200 mL of MeOH. Then iodine (I_2) (1.24 g, 4.87 mmol) was added to the reaction flask. Iodic acid (HIO_3) (660 mg, 3.75 mmol) was dissolved in 3 mL of water and added to the reaction mixture. The reaction mixture was stirred at 25 °C for 30 minutes. After the starting material was consumed, the MeOH was removed under reduced

pressure. The product was purified with a flash silica column using 50% ethyl acetate: hexane, (v/v) as the solvent system (50%).

Optical Measurement

A scanning spectrophotometer (Shimadzu UV-1800) was used to record UV-Vis absorption spectra of BODIPY compounds in the environment of THF solution. The fluorescence spectra of the studied compounds were measured with Perkin Elmer model LS 55 Fluorescence spectrometer.

Ultrafast pump-probe spectroscopy measurements were carried out to investigate the charge transfer dynamics of the studied compounds in THF. By using A Ti: Sapphire laser amplifier and an optical parametric amplifier system with 52 fs pulse duration and 1 kHz repetition rate (Spectra-Physics, Spitfire Pro XP, TOPAS), time and wavelength-dependent ultrafast pump-probe spectroscopy measurements were conducted in the femtosecond time window. A commercial pump-probe experimental setup (Spectra-Physics, Helios) with a white light continuum probe were used to reveal charge transfer dynamics of the investigated compounds both in solution and on film. Pulse duration was measured as 120 fs by cross-correlation inside the pump-probe setup. The pump wavelength for ultrafast pump-probe spectroscopy experiments was chosen based on the maximum absorption wavelength in linear absorption spectra. The excited-state dynamics were measured between 0.1 ps to 3.2 ns timescale. Surface Xplorer software from Ultrafast Systems was used to analyze the experimental data.

Computational Details

The possible geometries of compounds from the Gaussview 5.0 visualization program[43] were optimized in the Gaussian 09 W software package[44] by the DFT method with Becke's three parameters hybrid exchange-correlation functional (B3LYP) and Los Alamos National Laboratory 2 double- (Lanl2dz) basis set in the ground state.[45–47] Following that, we calculated the UV-Vis spectra, the FMO energies, the global chemical reactivity descriptors (GCRDs), and the binding energies (E_b) in the tetrahydrofuran (THF) solvent using the time-dependent density-functional theory (TD-DFT)/B3LYP with the Lanl2dz basis. We have also performed the density of states (DOS) diagrams and the inter-fragment charge transfer (IFCT) using the Gauss–Sum v3.0 program[48] and Multiwfn software,[40] respectively.

Conclusions

To investigate the effect of the conjugation phenyl ring and heavy iodine atoms on the steady-state absorption, emission spectra, and charge transfer dynamics, dye molecules with a functional-COOH group with or without a biphenyl ring at meso position and their compounds with heavy iodine atoms at −2, −6 positions of the BODIPY indacene core were synthesized. The linear absorption and emission spectra of the studied compounds in THF solution showed that there is a significant spectral red-shifting and fluorescence quenching upon binding the iodine atoms at −2, −6 positions of the BODIPY indacene core. The ultrafast transient absorption spectroscopy measurements proved that ISC occurred in the presence of iodine atoms. These results are ascribable to −2, −6 positions occupied by iodine atoms, which strongly influence the

efficiency of ISC between the lowest singlet (S_1) and triplet states, as well as the efficiency of fluorescence. The ISC rates were found to be 150 ps and 180 ps for compounds **B2** and **B4** chromophores, respectively. From the theoretical point of view, the IFCT results show that the intrinsic local excitation is responsible for high photoluminescence efficiency. We believe that the current work will be useful to researchers working on novel derivatives to find out about triplet photosensitizers.

Conflict of Interest

The authors declare no conflict of interest.

Data Availability Statement

The data that support the findings of this study are available from the corresponding author upon reasonable request.

[1] A. Kamkaew, S. H. Lim, H. B. Lee, L. V. Kiew, L. Y. Chung, K. Burgess, *Chem. Soc. Rev.* **2013**, *42*, 77–88.
[2] O. J. Stacey, S. J. A. Pope, *RSC Adv.* **2013**, *3*, 25550–25564.
[3] J. W. Tian, L. Ding, H. J. Xu, Z. Shen, H. X. Ju, L. Jia, L. Bao, J. S. Yu, *J. Am. Chem. Soc.* **2013**, *135*, 18850–18858.
[4] X. J. Jiang, J. T. F. Lau, Q. Wang, D. K. P. Ng, P. C. Lo, *Chem. Eur. J.* **2016**, *22*, 8273–8281.
[5] J. P. Liu, C. Z. Jin, B. Yuan, X. G. Liu, Y. Chen, L. N. Ji, H. Chao, *Chem. Commun.* **2017**, *53*, 2052–2055.
[6] R. Prieto-Montero, R. Sola-Llano, R. Montero, A. Longarte, T. Arbeloa, I. Lopez-Arbeloa, V. Martinez-Martinez, S. Lacombe, *Phys. Chem. Chem. Phys.* **2019**, *21*, 20403–20414.
[7] J. Xuan, W. J. Xiao, *Angew. Chem. Int. Ed.* **2012**, *51*, 6828–6838; *Angew. Chem.* **2012**, *124*, 6934–6944.
[8] L. Shi, W. J. Xia, *Chem. Soc. Rev.* **2012**, *41*, 7687–7697.
[9] D. Ravelli, M. Fagnoni, A. Albini, *Chem. Soc. Rev.* **2013**, *42*, 97–113.
[10] J. Z. Zhao, W. H. Wu, J. F. Sun, S. Guo, *Chem. Soc. Rev.* **2013**, *42*, 5323–5351.
[11] T. N. Singh-Rachford, F. N. Castellano, *Coord. Chem. Rev.* **2010**, *254*, 2560–2573.
[12] A. Monguzzi, R. Tubino, S. Hoseinkhani, M. Campione, F. Meinardi, *Phys. Chem. Chem. Phys.* **2012**, *14*, 4322–4332.
[13] D. B. Papkovsky, T. C. O'Riordan, *J. Fluoresc.* **2005**, *15*, 569–584.
[14] J. M. Lim, Z. S. Yoon, J. Y. Shin, K. S. Kim, M. C. Yoon, D. Kim, *Chem. Commun.* **2009**, *3*, 261–273.
[15] D. P. Specht, P. A. Martic, S. Farid, *Tetrahedron.* **1982**, *38*, 1203–1211.
[16] J. B. Borak, D. E. Falvey, *Photochem. Photobiol. Sci.* **2010**, *9*, 854–860.
[17] Y. Cakmak, S. Kolemen, S. Duman, Y. Dede, Y. Dolen, B. Kilic, Z. Kostereli, L. T. Yildirim, A. L. Dogan, D. Guc, E. U. Akkaya, *Angew. Chem. Int. Ed.* **2011**, *50*, 11937–11941; *Angew. Chem.* **2011**, *123*, 12143–12147.
[18] J. Z. Zhao, K. J. Xu, W. B. Yang, Z. J. Wang, F. F. Zhong, *Chem. Soc. Rev.* **2015**, *44*, 8904–8939.
[19] S. G. Awuah, Y. You, *RSC Adv.* **2012**, *2*, 11169–11183.
[20] X. S. Li, S. Kolemen, J. Yoon, E. U. Akkaya, *Adv. Funct. Mater.* **2017**, *27*.
[21] J. Z. Zhao, K. P. Chen, Y. Q. Hou, Y. Y. Che, L. Liu, D. Z. Jia, *Org. Biomol. Chem.* **2018**, *16*, 3692–3701.
[22] B. Kucukoz, G. Sevinc, E. Yildiz, A. Karatay, F. Zhong, H. Yilmaz, Y. Tutel, M. Hayvali, J. Zhao, H. G. Yaglioglu, *Phys. Chem. Chem. Phys.* **2016**, *18*, 13546–13553.
[23] A. Karatay, M. C. Miser, X. N. Cui, B. Kucukoz, H. Yilmaz, G. Sevinc, E. Akhuseyin, X. T. Wu, M. Hayvali, H. G. Yaglioglu, J. Z. Zhao, A. Elmali, *Dyes Pigm.* **2015**, *122*, 286–294.
[24] Y. Dong, A. Elmali, J. Z. Zhao, B. Dick, A. Karatay, *ChemPhysChem* **2020**, *21*, 1388–1401.
[25] Y. Dong, P. Kumar, P. Maity, I. Kurganskii, S. J. Li, A. Elmali, J. Z. Zhao, D. Escudero, H. J. Wu, A. Karatay, O. F. Mohammed, M. Fedin, *Phys. Chem. Chem. Phys.* **2021**, *23*, 8641–8652.
[26] F. M. Dumanogullari, Y. Tutel, B. Kucukoz, G. Sevinc, A. Karatay, H. Yilmaz, M. Hayvali, A. Elmali, *J. Photochem. Photobiol. A* **2019**, *373*, 116–121.
[27] E. Akhuseyin, O. Turkmen, B. Kucukoz, H. Yilmaz, A. Karatay, G. Sevinc, K. Xu, M. Hayvali, H. G. Yaglioglu, *Phys. Chem. Chem. Phys.* **2016**, *18*, 4451–4459.
[28] Y. M. Lee, R. M. Malamakal, D. M. Chenoweth, J. M. Anna, *J. Phys. Chem. Lett.* **2020**, *11*, 877–884.
[29] J. H. Zou, Z. H. Yin, K. K. Ding, Q. Y. Tang, J. W. Li, W. L. Si, J. J. Shao, Q. Zhang, W. Huang, X. C. Dong, *ACS Appl. Mater. Interfaces* **2017**, *9*, 32475–32481.
[30] C. Bellomo, D. Zanetti, F. Cardano, S. Sinha, M. Chaari, A. Fin, A. Maranzana, R. Nunez, M. Blangetti, C. Prandi, *Dyes Pigm.* **2021**, *194*.
[31] M. Obloza, L. Lapok, T. Pedzinski, K. M. Stadnicka, M. Nowakowska, *ChemPhysChem* **2019**, *20*, 2482–2497.
[32] T. Koopmans, *Physica.* **1933**, *1*, 104–113.
[33] M. Miar, A. Shiroudi, K. Pourshamsian, A. R. Oliaey, F. Hatamjafari, *J. Chem. Res.* **2021**, *45*, 147–158.
[34] S. Tekin, A. Karatay, D. Erdener, E. A. Yildiz, B. Boyacioglu, H. Ünver, M. Yıldız, A. Elmalı, *J. Mol. Struct..* **2022**, *1253*, 132239.
[35] S. Renuga, S. Muthu, *Spectrochim. Acta A Mol. Biomol. Spectrosc.* **2014**, *118*, 702–715.
[36] A. Srivastava, R. Mishra, P. Tandon, A. K. Bansal, *Spectrochim. Acta A Mol. Biomol. Spectrosc.* **2013**, *104*, 409–418.
[37] D. Madrid-Úsuga, A. G. Mora-Leon, A. M. Cabrera-Espinoza, B. Insuasty, A. Ortiz, *Comput. Theor. Chem..* **2021**, *1197*, 113165.
[38] J.-L. Bredas, *Mater. Horiz.* **2014**, *1*, 17–19.
[39] M. Mehrabpour, H. R. Shamlouei, H. Bahrami, *J. Mol. Model..* **2020**, *26*, 306.
[40] T. Lu, F. Chen, *J. Comput. Chem.* **2012**, *33*, 580–592.
[41] F. Sozmen, M. Kucukoflaz, M. Ergül, Z. D. Şahin İnan, Y. Bozkurt, D. Taydas, *Macromol. Res.* **2022**, *30*, 61–69.
[42] S. H. Lim, C. Thivierge, P. Nowak-Sliwinska, J. Y. Han, H. van den Bergh, G. Wagnieres, K. Burgess, H. B. Lee, *J. Med. Chem.* **2010**, *53*, 2865–2874.
[43] R. Dennington, T. Keith, J. Millam, "Gauss View Version 5," Semichem Inc., Shawnee Mission, **2009**.
[44] M. Frisch, G. Trucks, H. B. Schlegel, G. E. Scuseria, M. A. Robb, J. R. Cheeseman, G. Scalmani, V. Barone, B. Mennucci, G. Petersson, *Inc., Wallingford CT.* **2009**, *201*.
[45] A. Becke, *J. Chem. Phys.* **1993**, *98*, 5648.
[46] A. D. Becke, *J. Chem. Phys.* **1996**, *104*, 1040–1046.
[47] C. Lee, W. Yang, R. G. Parr, *Phys. Rev. B* **1988**, *37*, 785.
[48] N. M. O'boyle, A. L. Tenderholt, K. M. Langner, *J. Comput. Chem.* **2008**, *29*, 839–845.